Chapter 1
Introduction and Motivation

Chapter 1 presents an introduction to the luminescence phenomenon and its classification, the theory of phosphor materials and trivalent lanthanide elements, and the discussion of the various applications of phosphor materials. The current research in the field of white LED and fluorescence thermometry is also discussed in the chapter. At the end of the chapter motivation regarding thesis work is discussed.

1.1 General introduction to luminescence

Luminescence phenomena have mystified and thrilled humankind since ancient times. The glowing insects, colorful aurora, glowing fungus, and decaying wood are all examples of naturally occurring luminescent phenomena. The scientific study of luminescence phenomena started when in 1852 English physicist, Sir G. G. Stokes published his renowned article entitled "On the refrangibility of light" and gave his law of luminescence known as Stokes law, which states that the emitted radiation has a longer wavelength than the stimulating radiation. Then in 1888, German physicist and science historian, Eilhardt Wiedemann introduced the word luminescence for all the light emitting phenomena which are not generated by the rise in temperature. The term luminescence is derived from the Latin word lumen, meaning light. Thus, the luminescence phenomenon is defined as the emission of visible radiation from particular materials or organisms by chemical reactions, physiological processes, electrical energy, subatomic motion, or piezoelectricity. The luminescence phenomenon is different from incandescence as the latter results from heating. Although the luminescence phenomenon is not caused by heat, it is influenced by heat.

1.2 Classification of Luminescence phenomenon

The luminescence phenomena can be divided into several groups based on the manner of stimulation as described below and presented in Fig.1.1.

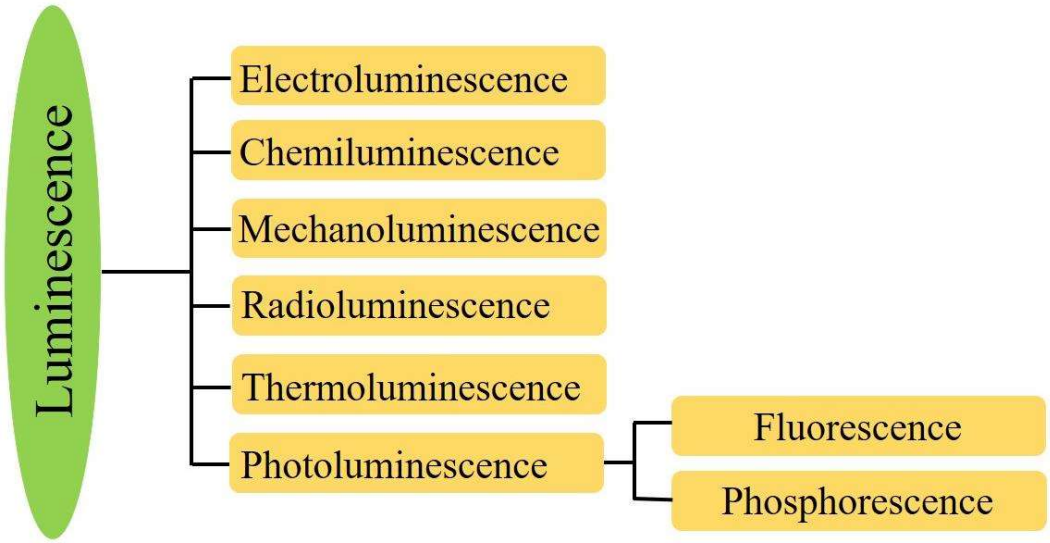

Fig. 1.1 Classification of luminescence processes based on Time duration and Excitation source.

The different source of excitation leads to different types of luminescence process as described below:

1.2.1 Electroluminescence

The optoelectronic phenomenon of the generation of photons when the material is stimulated by the passage of an electric current is called electroluminescence (EL). This process results from the radiative recombination of electrons and holes in the depletion region of the materials. The application of EL is in LEDs and electroluminescent displays.

1.2.2 Chemiluminescence

Chemiluminescence (CL) is the generation of electromagnetic (EM) radiation (Ultraviolet, visible, or infrared) by the process of electronic transition induced by certain chemical reactions. One type of CL is bioluminescence which results from the biochemical reactions in a living organism. In bioluminescence, less than 20% of light results in heat. Therefore, bioluminescence is also called cold light. There are many bioluminescent organisms such as fireflies and marine organisms.

1.2.3 Mechanoluminescence

Mechanoluminescence (ML) refers to the generation of radiation caused by any mechanical action on solids. The mechanical action can be in the form of cutting, compressing, rubbing, scratching, grinding, shaking, or cleaving. Thermal shocks created by severe cooling or heating of the specimen, or shock waves produced during sample exposure to strong laser pulses, can also stimulate ML. ML may also be seen during the deformation produced by the phase transitions or crystal development, as well as during the separation of two different materials in contact. Some of the different names given to the ML process depending on the type of mechanical action applied to the solid are piezoluminescence, triboluminescence, fractoluminescence, and sonoluminescence.

1.2.4 Radioluminescence

Radioluminescence (RL) is the process of production of EM radiation as a result of interaction between the ionizing particles (such as α particle, β particle, or γ rays) and matter. In RL the ionizing particles are the source of excitation. The materials which exhibit radioluminescence are called scintillators.

1.2.5 Thermoluminescence

Thermoluminescence (TL) of thermally stimulated luminescence is the process that involves heat as a source of excitation. In some crystalline solids, the electrons are previously trapped in the defects of the crystal structure. When a sufficient amount of thermal energy is imparted to these electrons, they become free and the trapped energy is emitted in the form of light, known as thermoluminescence. The information of the trap energies can be estimated by the emission curves. The applications of TL include archaeological dating and radiation dosimetry.

1.2.6 Photoluminescence

Photoluminescence (PL) is the luminescence phenomenon that involves incident photons as a source of excitation. PL spectroscopy is an important technique for determining the information regarding the electronic structure of the specimen, as well as its optical and photochemical characteristics and interfacial point defects. There are many important applications based on PL, such as fluorescent tubes and lamps, fluorescence microscopy, display devices, safety signs, counterfeit detection, phosphorescent paints, optical thermometers, and forensics. PL is further classified into two processes namely fluorescence and phosphorescence, depending on the emission lifetime.

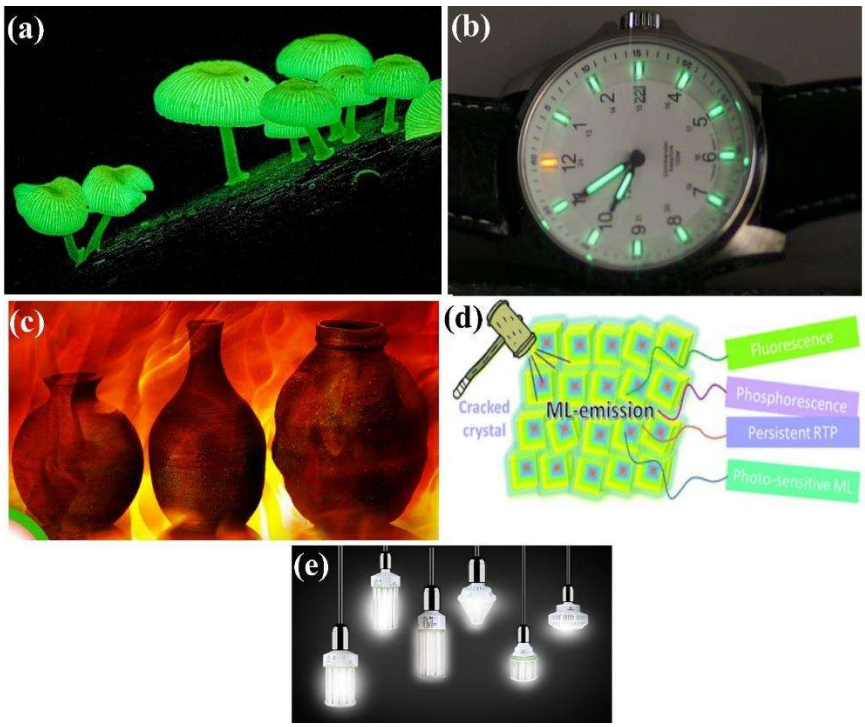

Fig. 1.2 (a) Bioluminescence in mushrooms **(b)** Watch face illuminated by tritium tubes **(c)** Thermoluminescence dating of ancient pots **(d)** Schematic representation of mechanoluminescence (ML) **(e)** Fluorescent LED bulbs.

As discussed earlier, photoluminescence is further classified into phosphorescence and fluorescence. In the 19th century, fluorescence was defined as an emission of light that diminishes with the end of stimulation, whereas phosphorescence is defined as the emission of light that continues beyond the end of excitation. However, this reasoning is inadequate

in understanding the two phenomena as there are long-lived fluorescence and short-lived phosphorescence whose durations are comparable.

1.2.6.1 Fluorescence

Fluorescence is the classification of photoluminescence where the absorption of incident photons by the molecule, initially in the singlet ground state, is prompted to a singlet excited state and as the excited molecule reverts to the ground state, it causes the emission of photons with a longer wavelength than the absorbed photons. The overall process of fluorescence takes 10^{-4} to 10^{-8} sec. The wavelength of emitted photons is always higher than the wavelength of absorbed photons. The spin multiplicity is retained in the fluorescence process, i.e., fluorescence does not interfere with the electron spin. Fluorescent dyes, paints, lamps, and biological markers are some of the applications of the fluorescence process.

1.2.6.2 Phosphorescence

Phosphorescence is also a type of photoluminescence which is a spin-forbidden process. In this process, the molecule is excited to a singlet excited state and then goes to an intermediate excited triplet state either by molecular collision or by intersystem crossing. The transition from the singlet to the triplet state involves spin reversal. The spin orientation in the excited triplet state and the ground state is the same, which makes the transition from triplet to singlet more improbable than single to singlet transitions. The transitions to the ground state are forbidden and the lifetime of the emission is more (10^{-3} to 10^{0} sec). Thus, phosphorescence is called delayed fluorescence. When exposed to light, the material exhibits a phosphorescence glow for a longer duration of time.

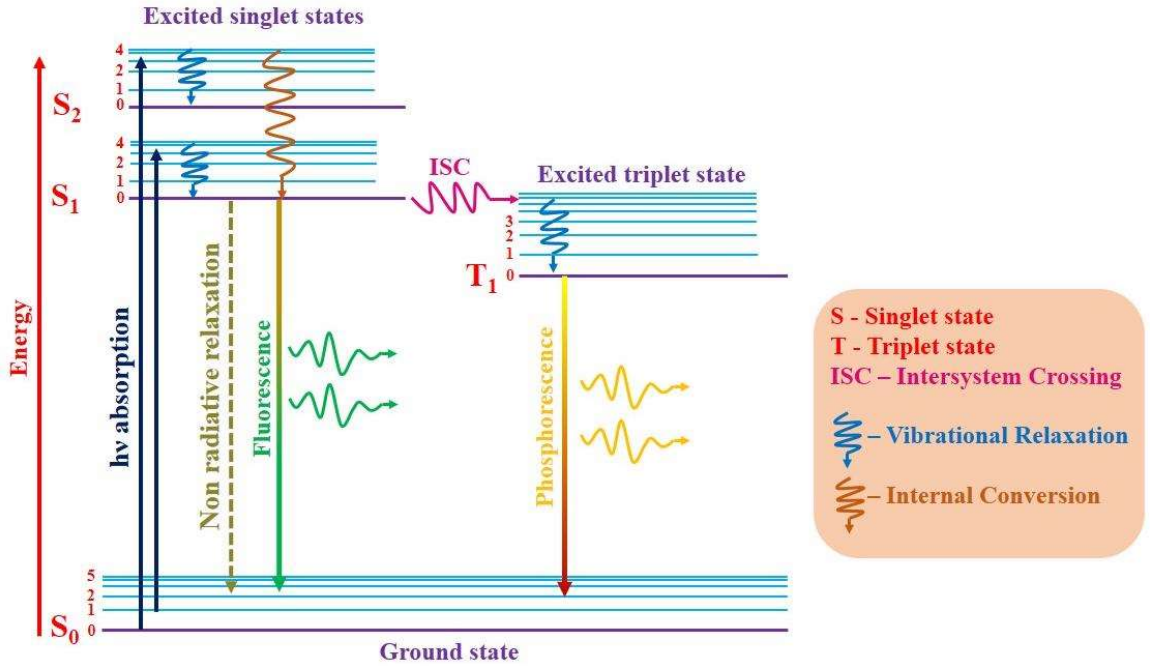

Fig. 1.3 Jablonski Diagram for explaining absorption, fluorescence, inter-system crossing, internal conversion, vibrational relaxation, and phosphorescence

1.3 Photoluminescence mechanism

All Materials exhibiting the luminescence property are usually referred to as *phosphors*. A synthesized phosphor material is usually composed of a suitable host crystal and doped impurities called luminescent centers or activator ions. The absorption of photon energy by the molecule results in its excitation, which subsequently results in relaxation. The relaxation of the molecule can lead to the emission of radiation. The emission can take place from the host lattice as well as from the dopant ions. The dopant ions in which an electron transition results in the emission of photons are called *activators*. In some cases, if the absorption of the activator ion is weak, an additional kind of dopant ion is co-doped in the lattice. This co-doped ion is called the *sensitizer* and it subsequently transfers the absorbed energy to the activator ion. The various processes involved in the phosphor material, starting from the absorption of photons to the emission of radiation are demonstrated by the Jablonski diagram. The Jablonski diagram is named after Professor Alexander Jablonski, who is widely recognized as the pioneer of fluorescence

spectroscopy. Fig. 1.3 depicts a typical Jablonski diagram, with the singlet ground and excited states labeled as S_0 and $S_{1,2}$, respectively. The vibrational energy levels are labeled as 0, 1, 2, etc. Typically, the energy of emission is smaller than that of absorption (Stokes law). The details of various processes are discussed as follows:

1.3.1 Excitation process

Electronic excitation refers to the electronic transition that occurs as a result of a photon being absorbed by a molecule. The excitation spectrum is recorded by examining emission at the wavelength of maximum intensity while the sample is scanned through a wavelength range. The excitation energy propels the molecule from the ground electronic state to a higher vibronic sublevel of an excited singlet state. The phosphors exhibit photoluminescence after the absorption from a suitable incident of electromagnetic radiation. The radiation is absorbed by the host lattice of the activator ion. If the radiation is absorbed by the host lattice, the emission occurs either from the host itself or via energy transfer from the host to the activator ion. In most cases, high energy radiations like far ultraviolet (UV) excite the host lattice and low energy radiations like near UV and visible light excite the activator ions. In some host phosphors, the activator ions exhibit weaker absorption. These host materials are doped with sensitizers which absorb energy and transfer it to the activator ions. The initial absorption process of the radiation takes place within a few femtoseconds.

1.3.2 Relaxation process

The relaxation of the electron from the excited state to the ground state is a spontaneous process. The relaxation involves both radiative and non-radiative transitions. The excited species dissipate energy via vibrational relaxation, internal conversion, intersystem crossing, fluorescence, and phosphorescence.

1.3.2.1 Radiative transition

If the relaxation of the activator ion from an electronically excited state to the ground state yields photon emission, then the transition is regarded as a radiative transition. The radiative transition may include transition from the excited singlet state to the ground singlet state or from the excited triplet state to the ground singlet state (Fig. 1.3). The transition from $S_1 \rightarrow S_0$ state (fluorescence) is allowed transition and takes about 10^{-8} sec. The transition between distinct states of multiplicity, such as the $T_1 \rightarrow S_0$ state (phosphorescence), is slower due to being forbidden. The two transitions follow stokes law which indicates that the released radiation has lower energy than the absorbed radiation. The radiative transitions are examined by examining the emission spectrum which is recorded by fixing the excitation wavelength, while the detection wavelength is scanned through the range of wavelengths.

1.3.2.2 Non-radiative transition

The energy absorption places a molecule in one of the higher vibrational states of one of its electronically excited states. Sometimes, an electron can return from the excited state to the ground state without emitting photons. This process is known as nonradiative relaxation. In the non-radiative relaxation process, the energy of the electron in the excited state is carried away by the phonons which are associated with the lattice vibrations of the host. The different types of non-radiative transitions are vibrational relaxation, internal conversion (IC), and intersystem crossing (ISC). IC is the non-radiative transition between energy states of the same spin state. The $S_2 \rightarrow S_1$ transition in Fig. 1.3 is an example of IC. The IC process is a spin-allowed transition and is, therefore, faster (10^{-12} sec or less). The vibrational relaxation process results in the electronically excited molecule in the lowest vibrational sublevels of the excited electronic state. The ISC is a non-radiative transition between states with differing spin multiplicity. The transition from the excited singlet state

to the excited triplet state is an example of ISC, Fig. 1.3. The ISC process is a spin-forbidden transition and is slower (10^{-8} – 10^{-3} sec).

1.3.3 Photoluminescence Decay Mechanisms

The average amount of time a fluorophore remains excited is referred to as its fluorescence lifetime. To further understand the meaning of fluorescence lifetime, let us suppose a sample containing several fluorophores. The excitation with an infinitely sharp pulse of light could result in the number of fluorophores reaching an excited state. Let n_0 be the initial population of fluorophores in the excited state. The population in the excited state decays with a rate of R+k_{nr} according to equation 1.1.

$$\frac{dn(t)}{dt} = (\mathrm{R} + k_{nr})\mathrm{n(t)} \tag{1.1}$$

Where R represents the emissive rate, the nonradiative decay rate is represented by k_{nr}, and the population of excited molecules following excitation at time t is denoted by $n(t)$[1]. An emission is a random event, and each stimulated fluorophore has the same probability of emitting in a given time. This causes the excited state population to decay exponentially,

$$n(t) = n_0 \exp(-t/\tau) \tag{1.2}$$

In a fluorescence experiment, the spectrophotometer records the fluorescence intensity, which is proportional to $n(t)$. Therefore, equation 1.2 takes the form as

$$I(t) = I_0 \exp(-t/\tau) \tag{1.3}$$

Where $I(t)$ is the time-dependent intensity, I_0 is the intensity at t=0, τ is the inverse of the total decay rate $(\mathrm{R} + k_{nr})$ [1]. The slope of the log $I(t)$ vs. t plot may be used to calculate the fluorescence lifetime.

In some samples, the fluorophores can decay by more than one process. Suppose there exist two Ln^{3+} ions in the sample such that there exists the process of energy transfer from one Ln^{3+} ion to another Ln^{3+} ion. Then the electrons in the excited state of one Ln^{3+} ion could have two decay times and the decay intensity after time *t* will follow the bi-exponential function,

$$I(t) = I_0 + B_1\, exp\left(-\frac{t}{\tau_1}\right) + B_2\, exp\left(-\frac{t}{\tau_2}\right) \quad (1.4)$$

Where τ_1 signifies fast decay time and τ_2 signifies slow decay time;

1.4 Phosphor materials

Phosphor (or luminescent) materials are the ones that exhibit the phenomenon of luminescence. The function of a phosphor is to convert incident radiation into visible photons. They are primarily composed of a host lattice with some dopants such as rare-earth or transition metal ions. The luminescence of the phosphor materials is primarily due to two mechanisms: luminescence of semiconductors and luminescence of localized centers. The first case usually happens following band-to-band excitation between impurity states formed in the bandgap (e.g., donor-acceptor pair luminescence in ZnS: Ag^+, Cl^-). Whereas, the luminescence of localized states results from the transitions between energy levels of single ions (e.g., 4f-4f transitions of Eu^{3+} in Y_2O_3:Eu^{3+})[2] or complex ions (e.g., the charge transfer transition of $[MoO_4]^{2-}$ in $CaMoO_4$)[3]. Some of the different host matrices are oxides[4,5], aluminates[6,7], silicates[8,9], phosphates[10,11], fluorides[12,13], tungstates[14,15], molybdates[16,17], vanadates[10,18], titanates[19], and many other complex lattices. Among these phosphors, some possess self-luminescence as a result of ligand-to-metal charge transfer (LMCT). Charge transfer from the molecular orbitals of the ligand to the vacant or partially filled metal d-orbitals results in the formation of the LMCT band. The doping of rare-earth

and transition metal ions allows tuning and shifting of the host luminescence as per the desired applications. Due to the sensitivity of the 5d orbitals to the surrounding crystal field, the host lattices have a considerable impact on rare-earth transitions, particularly the 5d-4f transition. The rigidity of the host lattice also is a significant factor in influencing thermally stable and efficient luminescence. It is because the rigidity of the host lattice would restrict the probability of the non-radiative transitions, thereby resulting in high thermal stability and quantum yield. The two host matrices used in the thesis work are $SrMoO_4$ and $Zn_3(VO_4)_2$ and the details of which are discussed in the sections below.

1.4.1 $SrMoO_4$ phosphor

Among various family of phosphor materials, the molybdates have drawn much attention because of various important factors such as simple and cheap raw materials, facile synthesis process, and high solubility for rare-earth dopants. These important factors allows the production of molybdate phosphor on an industrial scale. On the other hand, phosphors such as fluorides or nitrides require costly precursors and modified synthesis routes which could hinder their production on an industrial scale. The $SrMoO_4$ phosphor of the molybdate family has received a lot of attention among different molybdates owing to its excellent properties such as near-ultraviolet (UV) excitation, broadband emission in the visible region, excellent thermal and chemical stability, and high solubility for rare-earth ions, making it fitting for optoelectronic application [20,21]. The $SrMoO_4$ phosphor has the tetragonal crystal structure phosphors with the $I4_1/a$ space group. The crystal structure of $SrMoO_4$ is depicted in Fig. 1.4, where the structure is formed by SrO_8 dodecahedral and MoO_4 tetrahedron attached by Sr–O–Mo bonds.

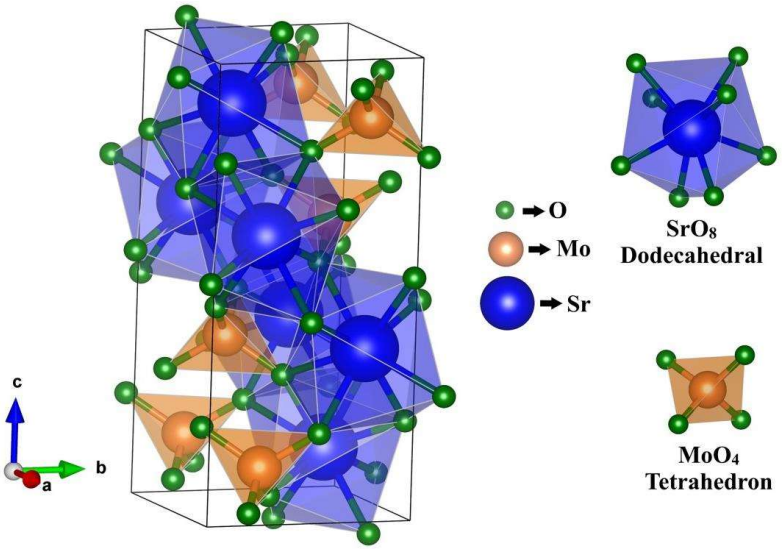

Fig. 1.4 Crystal structure of $SrMoO_4$.[22]

The $SrMoO_4$ phosphor is a self-activated luminescent phosphor that emits greenish-blue emission near UV excitation owing to the charge transfer between O^{2-} and Mo^{6+} in $[MoO_4]^{2-}$ groups [23,24]. The $O^{2-} \rightarrow Mo^{6+}$ charge transfer in $[MoO_4]^{2-}$ groups of $SrMoO_4$ causes the formation of LMCT (ligand to metal charge transfer) and MLCT (metal to ligand charge transfer) bands observed in the PLE and PL spectrum, respectively. A Typical excitation and emission spectrum of $SrMoO_4$ are presented in Fig. 1.5. The $SrMoO_4$ proves to be an excellent host for simultaneously transferring energy to different doped rare-earth ions. The role of $SrMoO_4$ host for optical thermometry application is discussed in chapter 5, where we have observe anti-thermal quenching phenomenon in the luminescence of Dy^{3+} doped $SrMoO_4$ which was then coupled with the usual thermal quenching occurring in Eu^{3+} doped $SrMoO_4$ for realization of effective dual-mode optical thermometry technique. This way we can see that the $SrMoO_4$ host can be utilized for multifunctional applications.

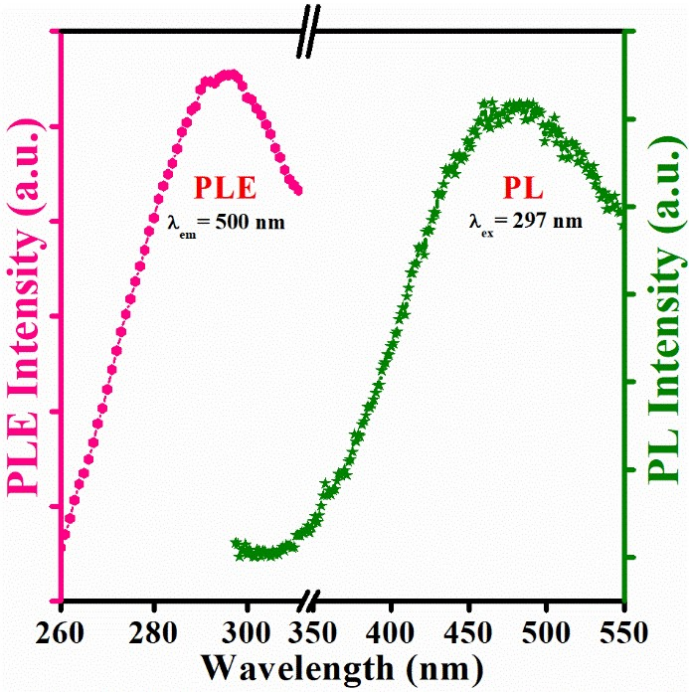

Fig. 1.5 Typical photoluminescence excitation and emission spectra of $SrMoO_4$ phosphor.[22]

1.4.2 $Zn_3(VO_4)_2$ phosphor

Zinc vanadate ($Zn_3(VO_4)_2$) phosphor comes from the family of $M_3V_2O_8$ (M= Zn, Ba, Sr, and Ca) vanadate system. Nakajima et al. have extensively studied the $M_3V_2O_8$ (M= Zn, Ba, Sr, and Ca) material system as well as the relationship between the structural characteristics and Quantum efficiency (QE) of $M_3V_2O_8$ vanadates with isolated VO_4 tetrahedra [25–27]. They determined that the weak connection between V^{5+} and M^{2+} ions, as well as the strong interaction between the V ions in the $M_3V_2O_8$ crystal structure, has a significant impact on the QE of these phosphors. The results from their research infer that in the family of $M_3V_2O_8$ phosphors, the $Zn_3(VO_4)_2$ phosphor has the best emission and QE. Furthermore, the QE of $Zn_3(VO_4)_2$ is better than several previously studied garnet vanadate phosphors [28]. Thus, the selection of $Zn_3(VO_4)_2$ over the other $M_3V_2O_8$ phosphors is obvious. The $Zn_3(VO_4)_2$ phosphors have an orthorhombic crystal structure with symmetry described by the space-group of Cmca. The V^{5+} ions occupy tetrahedral sites, whereas the Zn^{2+} ions occupy the two octahedral positions. The crystal structure of $Zn_3(VO_4)_2$ phosphor

is depicted in Fig. 1.6. The Zn^{2+} ions *m* and 2/*m* symmetry with three and two different bond lengths with oxygen, respectively.

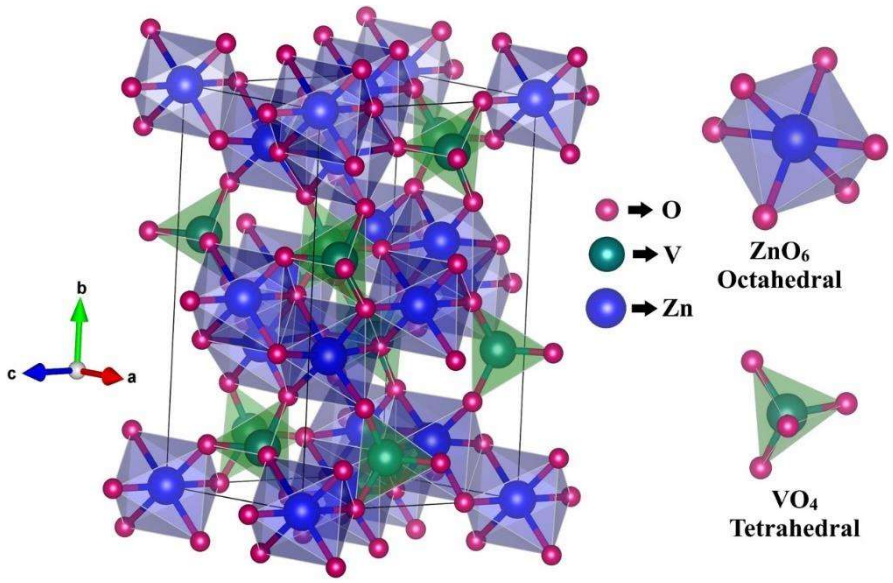

Fig. 1.6 Crystal structure of $Zn_3(VO_4)_2$.[29]

The self-luminescence feature of $Zn_3(VO_4)_2$ has made them preferable to commercial rare-earth-activated phosphors. The $Zn_3(VO_4)_2$ compound is stimulated with the near UV source and its emission spectrum covers the entire visible region [30–32]. The absorption of $Zn_3(VO_4)_2$ overlaps the emission spectrum of the commercially available near UV LED chips making it an ideal component for wLED devices [33,34]. The typical excitation and emission spectra of $Zn_3(VO_4)_2$ phosphor is shown in Fig. 1.7. The luminescence of the $Zn_3(VO_4)_2$ compound is owed to its VO_4 tetrahedral with T_d symmetry [30]. The charge transfer from 2p orbitals of O^{2-} to 3d orbitals of V^{5+} occurs in VO_4 tetrahedral, resulting in a broadband emission spectrum that encompasses the whole visible range [35]. This self-luminescence ability, together with a low-cost method of preparation and energy efficiency contributes to the advantage of $Zn_3(VO_4)_2$ over traditional phosphors [30–32].

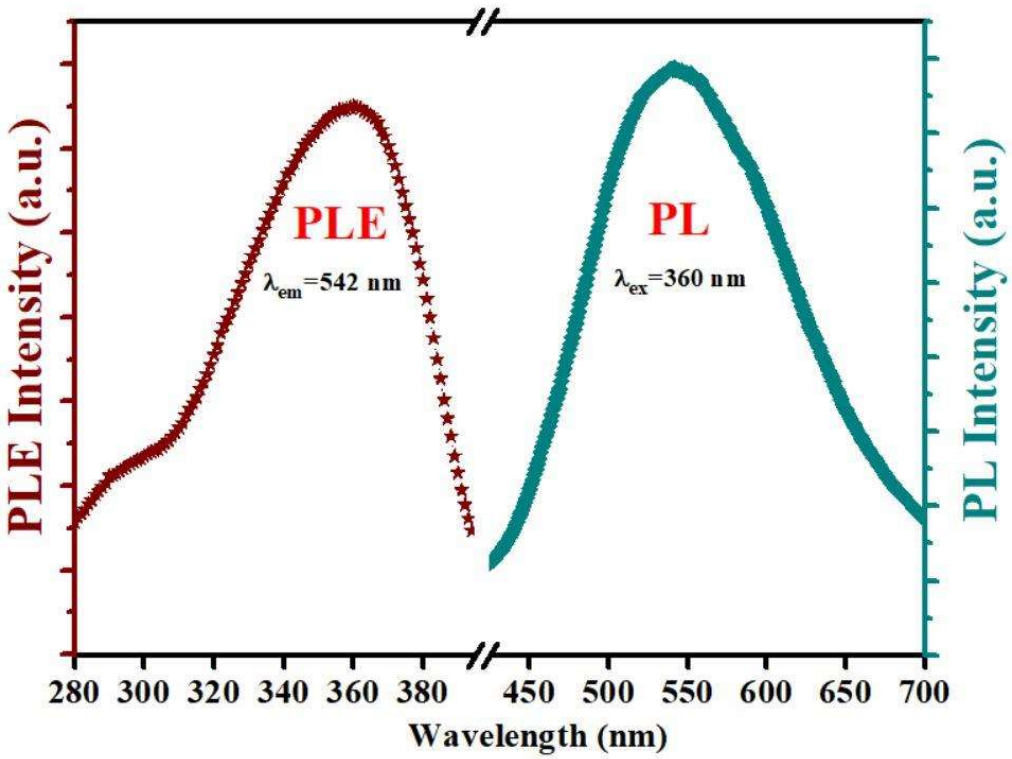

Fig. 1.7 Typical excitation and emission spectra of $Zn_3(VO_4)_2$ phosphor [36]

1.5 Rare-earth ions

The lanthanide (Ln) elements along with yttrium (Y) and scandium (Sc) are known as rare-earth (RE) elements. Despite cerium being the 25th most abundant element on earth, most of the RE elements are not found in concentrated or in pure form. The very scarcity of finding these elements in pure form and their incredible chemical similarities allowed them to be put in one family of RE elements. The fascinating optical properties of RE ions make them promising candidates for various emerging applications such as display devices, lighting devices, optical fibers, security and signage, solar energy converters, photo-catalysis, scintillators, bio-imaging, optical thermometry, and lasers [13,37–42]. The RE ions act as activators and co-activators in different host lattices and emit EM radiation in the UV, visible, and near-infrared (NIR) regions. The emission from RE ions is the result of unique optical transitions. The electronic configuration of Ln^{3+} ions is [Xe] $4f^n$ (n=0-14). These 4f electrons are well shielded from their environment by the closed $5s^2$ and $5p^6$ outer

shells. Each 4f electron is connected to one of the seven different 4f wavefunctions and the possible spin for it could be +1/2 or -1/2. The *n* number of electrons can be arranged in numerous ways into the seven 4f orbitals, which is called the degeneracy of the [Xe] $4f^n$ (n=0-14) configuration. Every unique electrical configuration is referred to as a microstate. Different perturbations operation on the Ln^{3+} ion partially or completely lift the degeneracy of the $4f^n$ configuration. These perturbations are crystal-field perturbations, spin-orbit coupling, electron repulsion, and the Zeeman Effect. The spin-orbit coupling is caused by the interaction of the electron's spin magnetic moment with the magnetic field formed by the electron's movement around the nucleus. The electron repulsion is the electrostatic interaction between the different electrons in the 4f shell. The Zeeman Effect results from the splitting of the energy levels caused by an external magnetic field. The interactions between the electrons of the 4f levels and the ligand generate the crystal-field effect. A spectroscopic term is defined by the two quantum numbers S (total spin quantum number) and L (total orbital angular momentum quantum number) while a spectroscopic level is additionally characterized by a third quantum number J (total angular momentum). The degeneracy of each spin-orbit level is 2J+1. The LS coupling scheme characterizes each free-ion level by $^{2S+1}L_j$. The crystal field effect lifts the 2J+1 degeneracy of the energy levels in the free ion even further, and the amount to which the degeneracy is eliminated depends on the symmetry class (cubic, icosahedral, tetragonal, hexagonal, octagonal, orthorhombic, pentagonal, monoclinic, trigonal, and triclinic) and the symmetry point group of the Ln^{3+} ion. These levels are called crystal field levels or the Stark levels. The degeneracy in the systems with orthorhombic or lower symmetry is lifted by the crystal field. Whereas, the degeneracy in the system with higher symmetry can be lifted by the application of an external magnetic field, via Zeeman Effect. Table 1 summarizes the total

number of terms, degeneracy, no of levels, ground level, and λ/cm^{-1} for f^n electronic configuration.

Table 1.1. The total number of terms, degeneracy, no of levels, ground level, and λ/cm^{-1} for f^n electronic configuration.

f^n		**Multiplicity**	**No of terms**	**No of levels**	**Ground level**		**λ/cm^{-1}**	
f^0	f^{14}	1	1	1	$^1S_0$	$^1S_0$	0	0
f^1	f^{13}	14	1	2	$^2F_{5/2}$	$^2F_{7/2}$	625	-2870
f^2	f^{12}	91	7	13	$^3H_4$	$^3H_6$	370	-1314
f^3	f^{11}	364	17	41	$^4I_{9/2}$	$^4I_{15/2}$	295	-793
f^4	f^{10}	1001	47	107	$^5I_4$	$^5I_8$	250	-535
f^5	f^9	2002	73	198	$^6H_{5/2}$	$^6H_{15/2}$	231	-386
f^6	f^8	3003	119	295	$^7F_0$	$^7F_6$	221	-285
f^7		3432	119	327	$^8S_{7/2}$		0	

In 1968, G. H. Dieke reported a comprehensive summary of the energy levels of the lanthanides and transitions [43,44]. The Dieke diagram, shown in Fig. 1.8, represents the energy levels of different lanthanides in the form of a term value ($^{2S+1}L_J$).

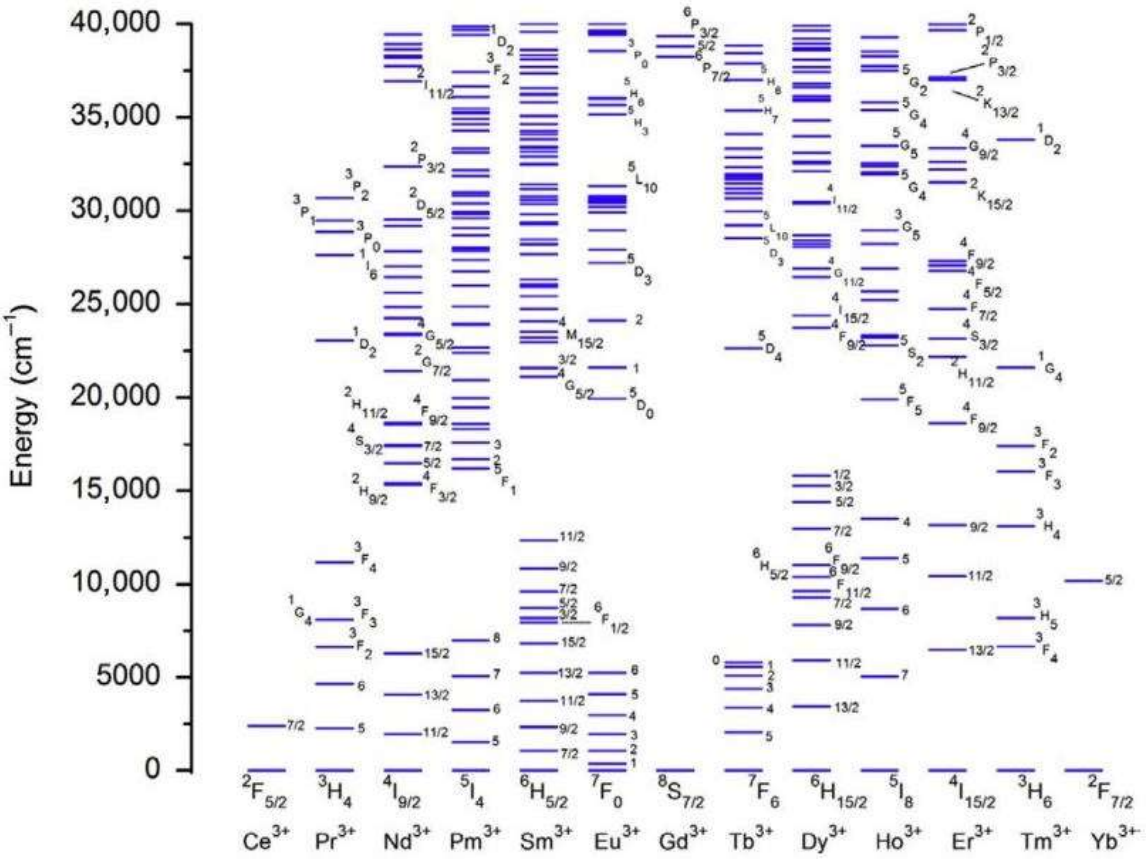

Fig. 1.8 Energy level structure of Ln^{3+} in the range up to 40,000 cm^{-1} [44].

Fundamentally, the Ln^{3+} ions exhibit three types of transitions including 4f-4f intra-configurational transition, 5d-4f inter-configurational transition, and the ligand to metal or metal to ligand charge transfer. These three types of transitions are discussed below.

1.5.1 4f-4f intra-configurational transition

The 4f-4f transitions involve the transfer of electrons among various energy states of 4f orbitals. The transitions observed in the luminescence spectrum of Ln^{3+} elements are either due to odd-parity electric dipole (ED) transitions or even-parity magnetic dipole (MD) transitions. An ED transition is a result of the interaction of the Ln ion with the electric field vector via an electric dipole, whereas, the MD transition is the consequence of Ln ion interaction with the magnetic field vector of the EM wave through a magnetic dipole. The intra-configurational ED transitions (e.g. s-s, p-p, d-d, and f-f) are forbidden by the *Laporte*

selection rule if the ground and excited states have the same symmetry with respect to an inversion center. However, when Ln ions are doped in the host lattice, they are influenced by the ligand field and the mixing of higher configurations into their 4f wavefunctions takes place. As a result, vibronic (vibrational-electronic) coupling takes place. This relaxes the Laporte rule and the ED transitions become partially allowed. Thus, the ED transitions are also called induced (or forced) ED transitions. The induced ED transitions are highly susceptible to the chemical environment around the Ln ion, therefore they are termed *hypersensitive* transitions. The MD transitions are parity-allowed. Their intensity is weak compared to the ED transitions. The MD transitions are largely insensitive to the environment around Ln ion. The selection rules determine whether an electronic transition is potentially allowed or forbidden. According to the selection rules from Judd-Ofelt theory, MD transitions obey $\Delta S = 0$, $\Delta L = 0$, and $\Delta J = 0, \pm 1$ whereas forced ED transitions obey $\Delta S = 0$; $\Delta L \leq 6$; $\Delta L = 2, 4, 6$ if L or $L' = 0$; $\Delta J \leq 6$; $\Delta J = 2, 4, 6$ if J or $J' = 0$. The higher order transitions such as electric quadrupole transitions are rarely observed in the Ln spectra. The f-f transitions give narrow emission bands as they are not affected by the surroundings because of shielding from 5s and 5p orbitals.

1.5.2 5d-4f inter-configurational transition

The inter-configurational 5d-4f transitions are allowed under a parity transformation. These transitions are allowed according to the Laporte rule. They feature broader bands than f-f transitions because of the large splitting of the 5d orbitals under the influence of crystal field strength. The emission from 4f-5d transitions can be easily tuned by varying the crystal composition and structure. Some rare-earth ions which exhibit 5d-4f transitions are Sm^{2+}, Ce^{3+}, Eu^{2+}, and Tb^{3+}.

1.5.3 Charge transfer transition

Charge transfer transition refers to the promotion of electrons into the excited energy levels of one atom or ion from the excited levels of another atom or ion within the same complex. The charge transfer involving the Ln ion can take place from the ligand to the Ln ion, between the two Ln ions, or from the central metal ion to the Ln ion in the same complex. The charge transfer transitions are Laporte-allowed transitions. A popular example is a $SrMoO_4:Sm^{3+}$ phosphor where the $O^{2+} \rightarrow Sm^{3+}$ charge transfer band occurs at 290 nm which is the result of a transfer of electrons from the p orbitals of O^{2+} to the partially-filled f orbitals of Sm^{3+} ions [45].

1.6 Trivalent Rare earth ions

1.6.1 Trivalent samarium ion

The trivalent samarium (Sm^{3+}) ion has five electrons in the outermost 4f shell and its electronic configuration is written as [Xe] $4f^5$. The emission spectrum of Sm^{3+} ions exhibits some intense peaks corresponding to the $^4G_{5/2} \rightarrow {}^6H_J$ (J=5/2, 7/2, 9/2, 11/2, and 13/2) electronic transitions. These electronic transitions give orange-red emission. Among these transitions, the $^4G_{5/2} \rightarrow {}^6H_{5/2}$ is purely magnetic dipole transition, the $^4G_{5/2} \rightarrow {}^6H_{7/2}$ transition is partly due to magnetic dipole transition and partly electric dipole transition, and $^4G_{5/2} \rightarrow {}^6H_{9/2}$ transition is purely electric dipole transition.

1.6.2 Trivalent dysprosium ion

The trivalent Dysprosium ion (Dy^{3+}) has [Xe] $4f^9$ electronic configuration [46]. The absorption spectrum of Dy^{3+} ion consists of sharp absorption peaks covering near UV to the visible region and attributed to $^6H_{15/2} \rightarrow {}^6P_{3/2}$, $^6P_{7/2}$, $^4I_{11/2}$, $^4I_{13/2}$, $^4G_{11/2}$, and $^4I_{15/2}$ electronic transitions. The emission spectrum of Dy^{3+} ion consists of peaks covering the blue to yellow region of the visible spectrum and attributed to $^4F_{9/2} \rightarrow {}^6H_J$ (J= 7/2, 9/2, 11/2,

13/2, and 15/2) and $^4I_{15/2} \rightarrow {}^6H_{15/2}$ electronic transitions. Among these, the $^4F_{9/2} \rightarrow {}^6H_{15/2}$ transition is the MD transition lying in the blue region, whereas the $^4F_{9/2} \rightarrow {}^6H_{13/2}$ transition is the ED transition lying in the yellow region. The $^4F_{9/2} \rightarrow {}^6H_{13/2}$ transition is hypersensitive and is affected by the environment around the Dy^{3+} ion. The Dy^{3+} ion is employed as an activator ion in various host materials for white light applications. The blue ($^4F_{9/2} \rightarrow {}^6H_{15/2}$) and yellow ($^4F_{9/2} \rightarrow {}^6H_{13/2}$) emission peaks combine to give white light emission. The emission from $^4I_{15/2}$ and $^4F_{9/2}$ can be used for temperature sensing applications as these two peaks are thermally coupled with an energy difference of around 991 cm^{-1} [46].

1.6.3 Trivalent europium ion

The trivalent europium ion (Eu^{3+}) has six electrons in the outermost 4f shell and its electronic configuration is written as [Xe] $4f^6$. The Eu^{3+} ion in several compounds exhibits intense luminescence owing to the $^5D_0 \rightarrow {}^7F_J$ (J=0 - 6) electronic transitions. The $^5D_0 \rightarrow {}^7F_0$ transition is strictly forbidden by the selection rules of the Judd-Ofelt theory. The occurrence of the $^5D_0 \rightarrow {}^7F_0$ transition indicates that the Eu^{3+} ion occupies C_{nv}, C_n, or C_s site symmetry in the lattice. The $^5D_0 \rightarrow {}^7F_1$ transition is a magnetic dipole (MD) transition and its intensity is largely independent of the environment around the Eu^{3+} ion. The $^5D_0 \rightarrow {}^7F_1$ transition is the direct consequence of the crystal field splitting of $^7F_1$. In compounds with centrosymmetric crystal structures, the intensity of the peak corresponding to the $^5D_0 \rightarrow {}^7F_1$ transition is most intense. The $^5D_0 \rightarrow {}^7F_2$ transition is the electric dipole transition whose intensity is significantly influenced by the local environment of the Eu^{3+} ion and therefore they are termed hypersensitive transitions. The intensity of the $^5D_0 \rightarrow {}^7F_2$ hypersensitive transition is often used as a measure for the asymmetry around the Eu^{3+} ion. Therefore, if the intensity of $^5D_0 \rightarrow {}^7F_2$ transition is maximum then the Eu^{3+} ion must have occupied the lower symmetry in the host lattice. The typical red luminescence of the Eu^{3+} ion is the consequence of the $^5D_0 \rightarrow {}^7F_2$ transition. The $^5D_0 \rightarrow {}^7F_3$ transition is generally very weak as

it is forbidden according to the Judd-Ofelt theory. $^5D_0 \rightarrow {}^7F_4$ transition is again an electric dipole transition. The dominance of the $^5D_0 \rightarrow {}^7F_4$ transition is an indication of D_{4d} symmetry in compounds. The other $^5D_0 \rightarrow {}^7F_5$ and $^5D_0 \rightarrow {}^7F_6$ transitions are rarely observed as they lie beyond 800 nm where the detectors of most spectrophotometers have low sensitivity. In some inorganic hosts, the luminescence from the Eu^{3+} ion can also originate from $^5D_1$, $^5D_2$, and $^5D_3$ levels. The characteristic peaks in the absorption spectra result from the $^7F_0 \rightarrow {}^5D_J$ (J=0, 1, 2) transitions. The Eu^{3+} doped compounds are explored for wide applications such as red phosphors in lighting and display applications, luminescent markers in biological applications, etc. Moreover, the spectra of the Eu^{3+} ion can also be used to probe the local symmetry around the rare-earth ion. The $^5D_0$ and $^5D_1$ energy levels of Eu^{3+} ion are thermally coupled levels and therefore, Eu^{3+} doped phosphors find application in optical thermometry.

1.6.4 Trivalent terbium ion

Terbium (III) is a green emitter and has been used in various electroluminescent devices. The strongest excitation peak of Tb^{3+} ions is observed at 368 nm, is accredited to $^7F_6 \rightarrow {}^5G_5$ transition. In emission spectra, there are various peaks observed owing to intraconfigurational electronic transitions. Main emissive lines are recorded at 488, 543, 585, and 619 that are accredited to $^5D_4 \rightarrow {}^7F_6$, $^5D_4 \rightarrow {}^7F_5$, $^5D_4 \rightarrow {}^7F_4$ and $^5D_4 \rightarrow {}^7F_3$ transitions correspondingly.

1.6.5 Trivalent holmium ion

Ho (III) rare-earth ion is a good luminescent center as it has various meta-stable multiplets. Trivalent holmium (III) ion is a green emitter that emits light from $^4F_4 + {}^5S_2$ energy level in the visible region. Excitation spectra of Ho^{3+} activated phosphors consist of four bands at

365, 382, 415, and 445 nm attributed to transitions from ground state $^5I_8$ to different excited states $^3H_5$, $^5G_4$, $^5G_5$ and $^5G_6$ respectively.

1.6.6 Trivalent erbium ion

Er(III) ion is an ideal rare-earth ion for red, green and blue upconversion phosphors. The two transitions of Er(III) at 800 nm ($^4I_{15/2} \rightarrow {}^4I_{9/2}$) and 980 nm ($^4I_{15/2} \rightarrow {}^4I_{11/2}$) can conventionally populate its metastable level $^4I_{9/2}$ and $^4I_{11/2}$ by low cost near infra-red laser diodes. Most investigations have been performed on Er^{+3} doped Y_2O_3 nanophosphors as it is a very efficient system for infra-red to visible up-conversion. Under 980 nm laser excitation, the emission spectra of Er^{3+}-activated phosphors show emissions in the green province 527–536 nm and 555–567 nm which are allocated to $^2H_{11/2} \rightarrow {}^4I_{15/2}$ and $^4S_{3/2} \rightarrow {}^4I_{15/2}$ transition, respectively.

1.6.7 Trivalent neodymium ion

Trivalent neodymium ion having $4f^3$ configuration shows absorption peaks from ground state $^{11}I_{9/2}$ to different excited energy levels in UV–Vis region. Under excitation at 473 nm ($^4I_{9/2} \rightarrow {}^5G_{5/2} + {}^2G_{7/2}$) characteristics infrared emission at 878, 1059 and 1333 nm was observed due to $^4F_{3/2} \rightarrow {}^4I_{9/2}$, $^4I_{11/2}$ and $^4I_{13/2}$ transitions correspondingly. Also, PL reveals that there were three emissive peaks ($^4F_{3/2} \rightarrow {}^4I_{9/2}$, $^4F_{3/2} \rightarrow {}^4I_{11/2}$ and $^4F_{3/2} \rightarrow {}^4I_{13/2}$) at 905, 1064 and 1335 nm on diode laser excitation at 808 nm. CIE study revealed the emission of orange color from Nd^{+3} doped phosphors.

1.7 Application of phosphor materials

The light-emitting property of phosphor materials is utilized in various lighting and display applications. One of the major applications of phosphor materials is white light emitting diodes (WLED), which have acquired a great share of the lighting market. With the improvement in efficiency and stability of WLEDs, many exciting and new applications

have been envisaged such as indoor farming, backlight units in liquid crystal displays, and phototherapy. The WLED application is discussed in detail in section 1.7.1.

Apart from the conventional lighting and display applications, the temperature sensing property of phosphor materials is currently utilized in diverse applications such as nanoscale temperature sensors for monitoring local temperatures and real-time temperature mapping to study various processes such as calcium signaling and protein folding [48,49], identification of "hotspots" in micro or nanoelectronics [50,51], biological applications such as biocompatible markers, photothermal therapies of tumors [37], and drug deliverers [52]. The temperature sensing property of phosphor material can also be used to detect the temperature of the harsh and corrosive environment where the conventional temperature sensors fail. The optical thermometry using phosphor materials is discussed in detail in section 1.7.2.

The phosphor materials also find its application in solar spectral converter for silicon-based solar cells, light conversion agent in functional plastic film to cover the greenhouse, drug delivery, and smart anti-counterfeiting applications.

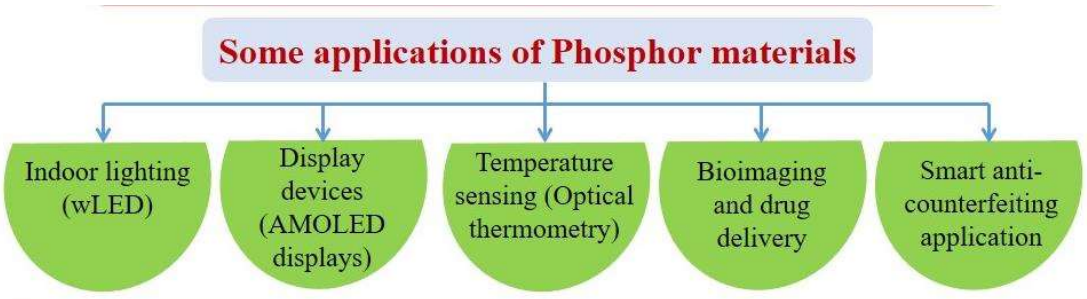

Fig. 1.9 Diverse applications of Phosphor materials

1.7.1 White Light Emitting Diodes

Solid state lighting devices such as phosphor-converted WLEDs have emerged as next-generation illumination sources and potential substitutes for traditional lighting devices such as halogen lamps, incandescent lamps, and fluorescent lamps. WLEDs have various

advantages over conventional light sources such as low power consumption (~8.5 W), high luminous efficiency (~100 lm W^{-1}), long operational lifetime (50,000 hours), high brightness (~800 lm), robustness, and environment-friendly characteristics (absence of mercury vapor) [39]. Currently, LEDs are utilized as key components in diverse applications, such as automotive lighting, medical applications, outdoor and indoor lighting at our homes, offices, and marketplaces, and display devices.

The first efficient WLED based on an InGaN chip coated with YAG:Ce^{3+} phosphor was developed by Y. Shimizu and co-workers at Nichia labs, which eventually started the WLED boom. Later, the fabrication of high-efficient blue-emitting LEDs by Isamu Akasaki, Shuji Nakamura, and Hiroshi Amano wave contributed to the improvement in the luminous efficacy of WLED from 25 ln W^{-1} to almost 200 ln W^{-1}. The blue light generated by the LED chip excites the yellow phosphor and the combination of yellow light (photoluminescence) and blue light (electroluminescence) gives the bluish-white light emission, as depicted in Fig. 1.10.

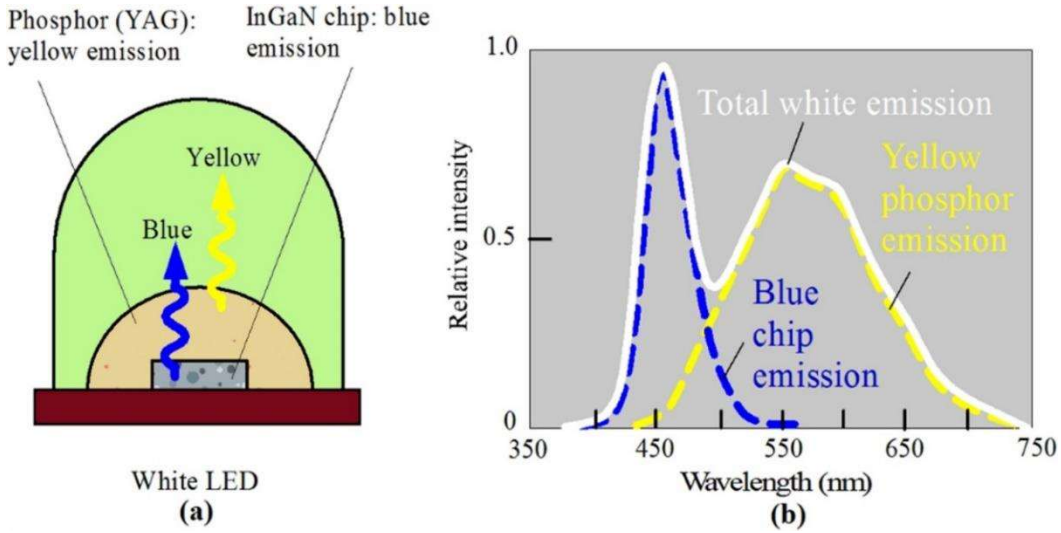

Fig. 1.10 (a) Fabrication of white LED based on yellow YAG:Ce^{3+} phosphor and blue InGaN chip. **(b)** Emission spectra of the commercial wLED.[53]

Currently, many commercially available WLED are fabricated in the same way which possesses good luminous efficacy (~150 lm W^{-1}). However, they suffer from poor color rendering index (CRI<75) and high correlated color temperature (CCT > 4,500 K) because of the absence of red-emitting material. To address this issue, tricolor (RGB) phosphors can be utilized to provide white light emission; however, this technology has various limitations, including light re-absorption, color ratio modification, and radiant inefficiency. The other way is by using red phosphors having near-UV/blue absorption. Various types of phosphors have been explored for their utilization as red phosphors in the LEDs, e.g., quantum dots, dyes, organic complexes, and inorganic phosphors with lanthanide ions as activators. The dyes and organic complexes have a broad near-UV/blue absorption band and high internal quantum efficiency (IQE) but they suffer from low thermal and chemical stability which hinder their application utilization. Quantum dots exhibit tunable and narrow emission bands (FWHM < 50 nm) but their composition is based on hazardous metals which is the major concern. Therefore, inorganic phosphors doped with lanthanide ions possess a certain advantage over other categories of phosphors as they are thermally and chemically stable and do not contain substantial concentrations of hazardous metals. Some of the inorganic red phosphors such as $Ca_3Si_2O_4N_2:Eu^{2+}$, $Sr[LiAl_3N_4]:Eu^{2+}$, $Ca_2Si_5N_8:Eu^{2+}$, $CaAlSiN_3:Eu^{2+}$, or $Sr_3Y_2Ge_3O_{12}:Eu^{2+}$, $Sr_2GeO_4:Eu^{2+}$, and yellow phosphor have been studied [54–58]. However, a major portion of the light produced by these phosphors is beyond the spectral sensitivity range of the human eye (i.e. beyond 700 nm), limiting its applicability in the field of wLEDs. Other constraints of these phosphors, such as the need for high temperatures and a limited environment for synthesis, necessitate large investments and restrict their practical applicability. Some of the desired properties of phosphor materials for WLED application are shown in Fig. 1.11.

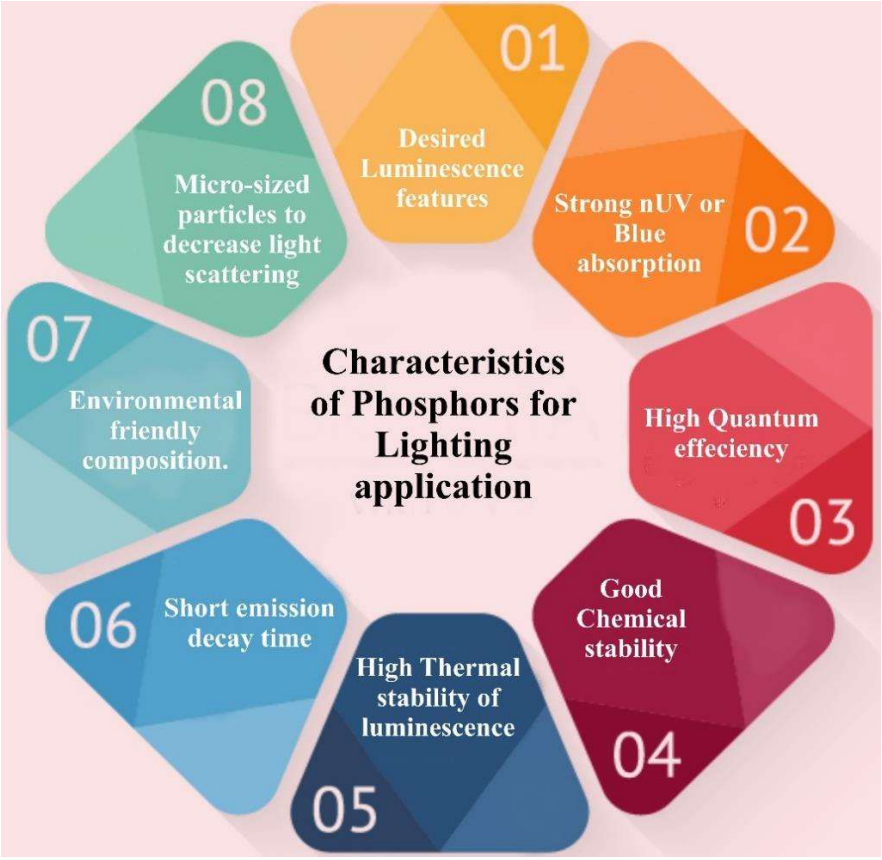

Fig. 1.11 Desired characteristics of phosphors for lighting applications.

1.7.2 Optical Thermometry

1.7.2.1 Temperature sensing techniques

Among all the physical parameters, temperature is one of the most studied parameter [59,60]. Reliable and accurate temperature sensing of the targets at desired scale plays a pivotal role in scientific research, climatology, manufacturing process in industries, and life activities. Temperature sensing accounts for about 80 % of the commercial sensor market [61]. Most of the traditional temperature sensors such as liquid-filled thermometers, bimetallic thermometers, thermistors, and thermocouples, are based on the principle of thermal expansion of liquids/metals or temperature-induced variation in resistance or voltage. However, all these traditional sensors require direct contact with the target which limits the use of these sensors in harsh and corrosive environments. Moreover, they are not immune

to electromagnetic interference, and the heating of the components may lead to inaccurate measurements [62,63].

The limitations of the traditional temperature sensors have greatly accelerated the emergence of non-invasive temperature sensing techniques with high thermal resolutions. Some of the non-invasive temperature sensing techniques are infrared (IR) thermography, thermometry-based Raman spectroscopy, thermo-reflectance, and fluorescence thermometry [64–66]. IR temperature sensing devices suffer from various limitations such as low spatial resolution, large temperature uncertainty (~1 K at room temp.), and they provide temperature distributions of the surface of the target only [67]. Raman spectroscopy on the other hand could be used to probe temperature at micron level but it has low signal levels and crosstalk with fluorescent molecules [67]. Various kinds of temperature sensing devices and methods based on contact and non-contact methods are presented in Fig. 1.12.

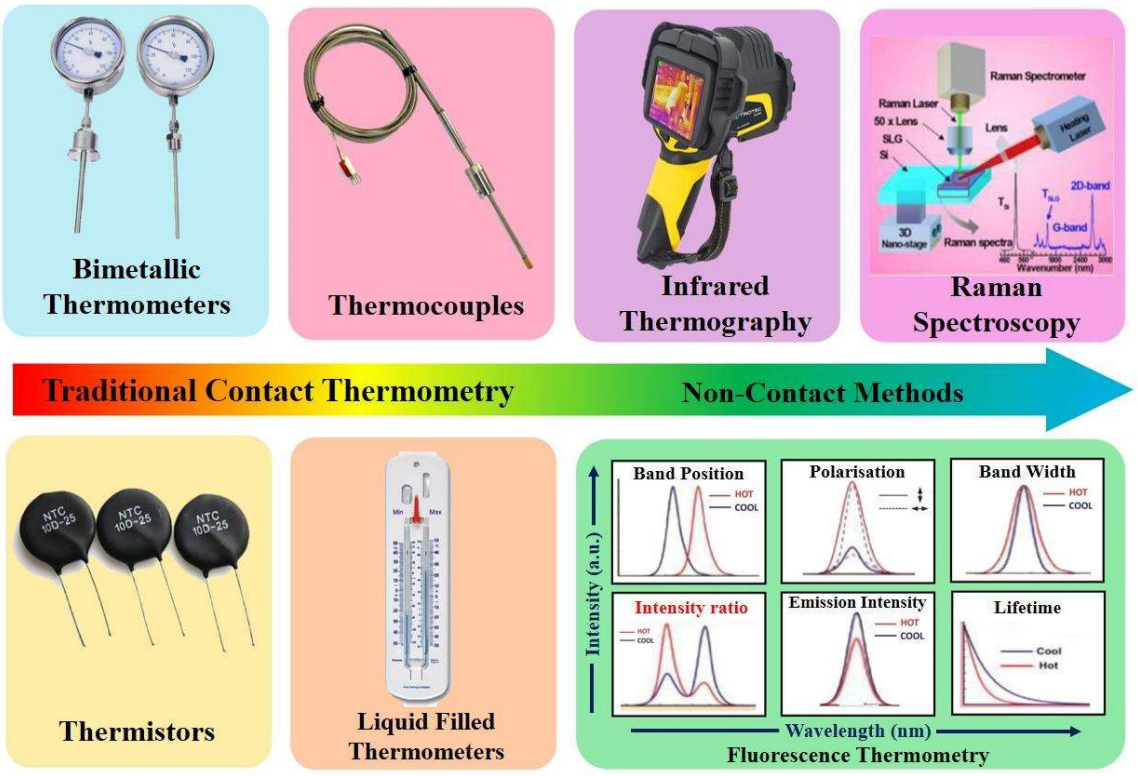

Fig. 1.12 Various temperature sensing techniques based on contact and non-contact mode of operation.

1.7.2.2 Fluorescence thermometry

Fluorescence thermometry is a kind of non-invasive temperature sensing technique that is based on thermo-responsive spectral parameters. Fluorescence thermometry alleviates the problems inherent with traditional temperature sensor systems as it provides a non-invasive mode of operation, electromagnetic passivity, fast response, remote readouts, and high-temperature sensitivity. Significant efforts have been made to explore and design novel optical materials as potential thermal probes. These optical materials include Ln^{3+} ions, organic dyes, quantum dots, protein and DNA conjugated systems, polymers, and hybrid materials [42,61,68–71]. Among these optical materials, the Ln^{3+} doped inorganic phosphors received a great deal of attention owing to their numerous advantages such as excellent luminescence properties, low toxicity, superior thermal and chemical stability, and narrow bandwidth. There are different temperature-dependent spectral parameters such as spectral position, polarization, fluorescence intensity ratio (FIR), fluorescence lifetime, and bandwidth that can be adopted to determine temperature, as shown in Fig. 1.8 [72]. Among these parameters, temperature sensing based on the absolute intensity from a single transition is affected by phosphor concentration, fluctuations in excitation source, and spectrum loss. These obstacles can be overcome using PL lifetime as a thermometric parameter, yet PL lifetime measurements are difficult for thermal dynamic study and they are time-consuming as well. Other parameters such as line broadening or shift are less induced by temperature, resulting in low thermal sensitivity. On the other hand, the fluorescence intensity ratio, also known as self-referencing ratiometric fluorescence thermometry, could well overcome the technical hurdles by examining the temperature-induced variations of the two emission peaks from single or dual fluorescent emitters. This reduces the dependence on measurement conditions, such as excitation intensity fluctuations, spectrum loss, and electromagnetic compatibility problems.

1.7.2.3 FIR thermometry

The FIR thermometry relies on the changes in the relative intensities of the two thermally coupled energy levels (TCELs) of an Ln^{3+} ion. Kusama et al. were the first to propose temperature measurements based on the FIR produced by the transition of two energy levels [73]. Later, Shinn et al. reported the theoretical expression of temperature measurement based on the FIR method applied to TCELs of Er^{3+} ion [74]. After a few years, Berthou et al. achieved temperature sensing in 293 K – 493 K by using Er^{3+} ions [75]. The FIR-based technique has developed over the years and in 2010, it was applied to single-cell intracellular temperature measurement [76]. Over the years now, FIR-based thermometry has been improved and applied to diverse applications [77,78]. Some of the Ln^{3+} ions which have TCELs are Eu^{3+} ($^5D_0$ and $^5D_1$) [79], Dy^{3+} ($^4I_{15/2}$ and $^4F_{9/2}$) [14], Er^{3+} ($^2H_{11/2}$ and $^4S_{3/2}$) [5], and Nd^{3+} ($^4F_{5/2}$ and $^4F_{3/2}$) [80], shown in Fig. 1.13.

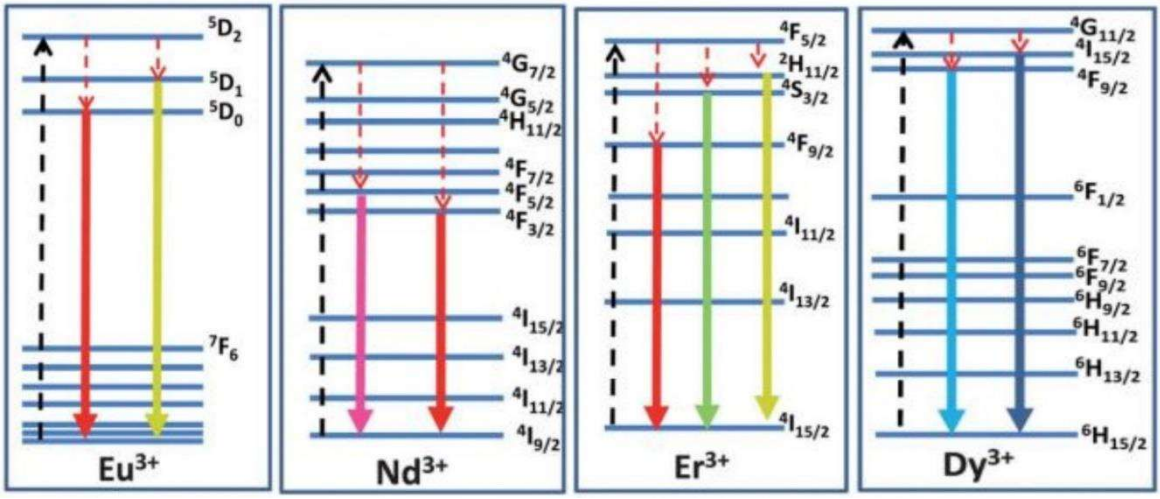

Fig. 1.13 Energy level diagrams of some trivalent lanthanide ions having TCELs.

The TCEL-based FIR thermometry relies on the rapid particle exchange between the two thermally coupled excited levels of Ln^{3+} ion. For the rapid particle exchange to take place, it is required that the energy gap (ΔE) between the two levels should be in the 200 – 2000 cm^{-1} range. At this small energy separation (i.e. comparable to the thermal energy k_BT),

with the rise in temperature, the population of the particles will not be restricted to a single energy level and it will be re-distributed between the TCELs. The single Ln^{3+} emitter-based FIR thermometry scheme is shown in Fig. 5. The two TCELs of the Ln^{3+} ion are labeled as 1 and 2. After the optical excitation the energy level labeled as 1 is populated (N_1). However, because of the proximity of a second energy level (level 2), the population is thermally re-distributed between the two levels. The population of level 2 (N_2) in steady state condition is given by equation 1.5,

$$N_2 = N_1 exp(-\Delta E/k_B T) \tag{1.5}$$

Due to the distribution of the population at both levels, emission also occurs from both levels. The luminescence intensity corresponding to the de-excitations from level 1 and level 2 are is given by,

$$I_1 = \varphi_1 N_1 \tag{1.6}$$

$$I_2 = \varphi_2 N_2 \tag{1.7}$$

Where φ_1 and φ_2 are the constants which depend on the intrinsic properties of the excited energy level. Thus, the ratio between both intensities is given by equation 1.8,

$$FIR\left({}^{I_2}/_{I_1}\right) = (\varphi_2/\varphi_1)(N_2/N_1) = (\varphi_2/\varphi_1)exp(-\Delta E/k_B T) \tag{1.8}$$

Therefore, a temperature can be determined by experimentally calculating the FIR. We can further investigate the thermal sensitivity by evaluating the absolute and relative sensitivity (S_a and S_r) using equations 1.9 and 1.10,

$$S_a = \left|\frac{\partial FIR}{\partial T}\right| = Cexp(-\Delta E/kT) \times \frac{\Delta E}{kT^2} \tag{1.9}$$

$$S_r = \left|\frac{1}{FIR}\frac{\partial FIR}{\partial T}\right| \times 100\% \tag{1.10}$$

Where the relative sensitivity is independent of the operational principle of thermometry and represents the relative change of the FIR per degree of temperature change (in % K^{-1}), i.e. FIR ratio. Since for a particular Ln^{3+} ion, the value of ΔE of the two monitoring energy levels is fixed, therefore the dependence of S_r on the ΔE restricts its upper limit[81]. As a result, the conventional single Ln^{3+} emitter-based FIR thermometry exhibits relatively low S_r values (1% or lower) [82]. Lower S_r values hinder the accuracy of temperature measurement and do not meet the requirements of various applications such as clinical medicine. Moreover, the low ΔE values would result in the overlapping of the two monitoring peaks, which results in inferior signal discriminability [83,84]. However, if materials are chosen with wide ΔE values, it could result in better signal discriminability and higher S_r values but simultaneously weakens the thermal coupling of TCELs, leading to lower S_a values [85,86]. Therefore, in a single Ln^{3+} emitter-based FIR method it is impossible to simultaneously promote S_r, S_a, and signal discriminability.

To overcome the limitations of the single Ln^{3+} emitter-based FIR method, a dual emitting center (Ln^{3+}- Ln^{3+}) is designed as an FIR-based temperature probe [83,84,86]. The temperature sensing mechanism in dual emitting center-based FIR can be illustrated by the use of Arrhenius equation [87],

$$I_a(T) = \frac{I_{a,0}}{1+D_a \exp\left(\frac{-E_a}{k_B T}\right)} \tag{1.11}$$

And,

$$I_b(T) = \frac{I_{b,0}}{1+D_b \exp\left(\frac{-E_b}{k_B T}\right)} \tag{1.12}$$

$$FIR\left(\frac{I_a(T)}{I_b(T)}\right) = \frac{I_{a,0}}{I_{b,0}} \frac{1+D_a \exp\left(\frac{-E_a}{k_B T}\right)}{1+D_b \exp\left(\frac{-E_b}{k_B T}\right)} \sim \alpha + \beta \exp\left(\frac{-\Delta E}{k_B T}\right) \tag{1.13}$$

Where α and β are the parameters associated with $I_{a,0}/I_{b,0}$ and D_b/D_a, respectively[87]. Furthermore, for better signal detection, the monitoring energy levels of the two Ln^{3+} ions should be far from each other. The S_a and S_r values can be calculated by equations 1.9 and 1.10. The two Ln^{3+} ions used in the dual emitting based FIR thermometry can be effectively excited by the metal to metal inter-valence charge transfer from the metal ions (Mo^{6+}, Nb^{5+}, W^{6+}, Ti^{4+}, or V^{5+}) of the host phosphor to the doped Ln^{3+} ions[88–90].

1.8 Motivation of the thesis

The thesis work is directed along the luminescence study of rare-earth ions doped $SrMoO_4$ and bismuth and lithium-doped $Zn_3(VO_4)_2$ phosphors. The limitations of the commercially available WLEDs such as high correlated color temperature (CCT > 4,500 K) and limited color rendering index (CRI<75) have motivated many researchers to develop red phosphors for the generation of warm white light. Although many researchers have studied various red phosphors for lighting applications, their limitations such as the need of high temperature and reduced atmosphere for synthesis, low thermal and chemical stability, and emission lying beyond 700 nm have motivated us to synthesize red phosphors which could be developed by low-cost and an environmentally friendly preparation method with good chemical and thermal stability. Moreover, it is also well studied that the emission intensity of RE ions can be increased by co-doping different alkali (Li^+, K^+, Na^+), bismuth (Bi^{3+}) ions, and transition metal ions (Mn^{2+}, Zn^{2+}, etc). The relatively small ionic radius of dopants allows them to easily occupy the substitutional or interstitial positions and by increasing the asymmetry they alter the crystal field around the RE ion. These ions also result in improved crystallinity and reduced defect states. All of these factors contribute to an increase in the luminescence intensity of RE ions. Therefore, we have examined the effect of Zn^{2+} and Bi^{3+} ions on the optical and structural properties of Sm^{3+} doped $SrMoO_4$

red phosphor. We have also examined the thermal stability of the best-prepared red phosphor and compared our results with some of the previously reported work.

The $SrMoO_4$ phosphor as a host is an excellent host for Ln^{3+} ions as it allows efficient and simultaneous energy transfer from the host LMCT band to the energy levels of the doped rare-earth ions. Therefore, it is possible to get a good emission corresponding to the two rare-earth ions when the phosphor is excited with the host excitation. We have utilized this property of $SrMoO_4$ phosphor for dual emitting center FIR thermometry. For this purpose, we have doped Dy^{3+} and Eu^{3+} ions in the $SrMoO_4$ phosphor and evaluated the relative sensitivity of the phosphor. We obtained excellent relative sensitivity and compared our results with the other reported phosphors. The use of dual emitting centers has also resulted in excellent color discriminability, which is also important for optical thermometry applications. Apart from optical thermometry, we have also explored the Dy^{3+}/Eu^{3+} co-doped $SrMoO_4$ phosphor for tunable color sources. The use of a tunable light source in a variety of applications such as multicolor display devices, encrypted information storage, white light-emitting diode (wLED), biological applications, and fluorescent sensors have motivated us to work in this field. We have obtained color tunability by precisely controlling the contents of Dy^{3+} and Eu^{3+} ions and by modulation of excitation wavelength.

To explore vanadate phosphors as an alternative to the commercially available yellow phosphor, we have studied zinc vanadate phosphor. Vanadate phosphors have self-luminescence property owing to the charge transfer from 2p orbitals of O^{2-} to 3d orbitals of V^{5+}. They also have near UV absorption which overlaps with the emission of commercially available near UV LED chips. Moreover, vanadate phosphors can be synthesized by a low-cost synthesis process. Among different phosphors of the $M_3V_2O_8$ (M= Sr, Ba, Zn, and Ca) family, the $Zn_3(VO_4)_2$ phosphor has the highest reported emission and quantum efficiency.

However, there were very few reports on single-phase $Zn_3(VO_4)_2$ phosphor. We have successfully prepared the single-phase $Zn_3(VO_4)_2$ phosphor and investigated the effect of bismuth and lithium on the luminescence of the phosphor. We have also studied the thermal stability of lithium-doped $Zn_3(VO_4)_2$ phosphor and compared the result with the other reported vanadate phosphors.